The Performance of High-Frequency Doppler Sonars in Actively Breaking Wave Crests

Grant B. Deane

***Abstract*—Breaking ocean waves influence wave dynamics, momentum transfer, air–sea exchange, ocean albedo, and ambient noise generation, all of which are impacted by the transient, two-phase flow in a whitecap. Lasting O(1s) or so, actively breaking whitecaps contain air fractions up to 0.6, bubbles ranging in size O(10–1000) μm and turbulent dissipation rates O(1) W·kg^{-1}. Strong fluid turbulence, high air fractions, large bubbles, and short duration make active whitecaps a challenging process to study. This paper presents a model for the performance of high-frequency Doppler sonar (0.5–2 MHz) when used to probe the interior of actively breaking whitecaps. The results suggest that the ability of high-frequency sonars to penetrate the interior of bubble plumes in whitecaps becomes limited for air fractions greater than 0.03–0.06 and plumes become completely impenetrable for air fractions greater than 0.08–0.17. This severely limits their usefulness as a tool to probe the interior of breaking waves. Moreover, the bias introduced by the terminal rise velocity of large bubbles interacting with fluid turbulence within the wave crest will need to be accounted for when interpreting any backscatter signals that are returned from the plume interior. At this time, *in situ* methods such as optical fiber probes, conductivity cells, and cameras remain the best option for field studies of the interior of breaking oceanic waves.**

***Index Terms*—Bubble plumes, Doppler sonar, turbulence, wave breaking.**

I. Introduction

WAVE BREAKING at the sea surface is an important process that limits wave height, transfers momentum into the upper ocean, and generates turbulence in the wave-affected surface layer [1]. Moreover, air entrained by breaking waves in the form of bubbles enhances the air–sea transfer of gases, generates marine aerosol and underwater noise, and increases ocean albedo. Fluid turbulence and air entrainment occur simultaneously in actively breaking wave crests,[1] where dissipation rates measured in the laboratory can exceed 1 W $\cdot$ kg^{-1} [2] and air fractions α measured in the field and laboratory reach values of 0.6 [3]–[6]. Despite its importance, little is known about the time-evolving behavior of the transient, energetic, two-phase flow generated by wave breaking and its dependence on the scale and slope of the breaking crest. Field observations of the interior of breaking crests are extremely challenging and there are few published data. Bezzabotnov et al. appear to have reported the first field observations of bubbles in whitecaps using an *in situ* camera system [7]. Two additional data sets of bubble distributions in actively breaking oceanic wave crests have been published by Bowyer [8] and Deane and Stokes [9] who also used *in situ* imaging. Note that we are excluding here the many observations of bubbles in the upper ocean boundary layer away from actively breaking wave crests, which are orders of magnitude lower in air fraction and do not contain millimeter-scale (mm-scale) bubbles. The only field observations of fluid turbulence in actively breaking wave crests in the field appear to be those of Gemmrich [10], who used a 2-MHz Doppler sonar system to measure turbulence within and beneath breaking waves on a wind-driven lake.

Given the difficulty of *in situ* observations of the interior of breaking waves in wind-driven seas, a potentially attractive instrument for probing breaking crests is the high-frequency acoustic Doppler sonar. Mounted below the wave-affected surface layer and pointed upwards, this instrument reports the density and velocity of scattering centers in horizontally stacked layers through the analysis of Doppler-shifted, backscattered acoustic pulses. High-frequency Doppler sonars have proven to be sensitive and useful sensors of fluid motions, surface waves, and bubbles in the upper ocean boundary layer for low [$\alpha < O(10^{-5})$] air fractions [4], [11]–[16]. If high-frequency sonar pulses can penetrate into the two-phase flow in a breaking crest, then it might also serve as a remote sensing probe of that flow, providing valuable information about fluid turbulence during active breaking in addition to flow structure and bubbles at greater depths and after active breaking.

Here we distinguish between bubble plumes and bubble clouds. Bubble plumes are composed of a high air fraction, transient, two-phase flow that occurs during active wave breaking. Bubble clouds are the remnants of plumes, and consist of patches of bubbles and turbulence left behind after a wave breaks. Bubble clouds are organized by upper ocean turbulence driven by waves, Langmuir cells and convective instabilities, and they evolve under the forces of advection, diffusion, buoyancy, and dissolution. They are in general much larger than bubble plumes and, because buoyancy removes large bubbles from plumes soon after active breaking ends, they have air fractions that are orders of magnitude lower and contain bubbles that are orders of magnitude smaller. A useful demarcation between bubble plumes and clouds can be based on the sounds of air entrainment. If a breaking wave crest generates the sounds of newly formed bubbles, then it is classified as a bubble plume.

Manuscript received June 02, 2015; revised October 07, 2015; accepted January 20, 2016. Date of publication April 04, 2016; date of current version October 11, 2016. This work was supported by the National Science Foundation under Grant OCE-1061050 and the Office of Naval Research under Grant N00014-14-1-0213.

Associate Editor: L. Culver.

The author is with the Marine Physical Laboratory, Scripps Institution of Oceanography, University of California San Diego (UCSD), La Jolla, CA 92023-0238 USA (e-mail: gdeane@ucsd.edu).

Digital Object Identifier 10.1109/JOE.2016.2521247

[1]By the term "actively breaking," we mean wave crests that are actively entraining air bubbles and therefore generating underwater noise.

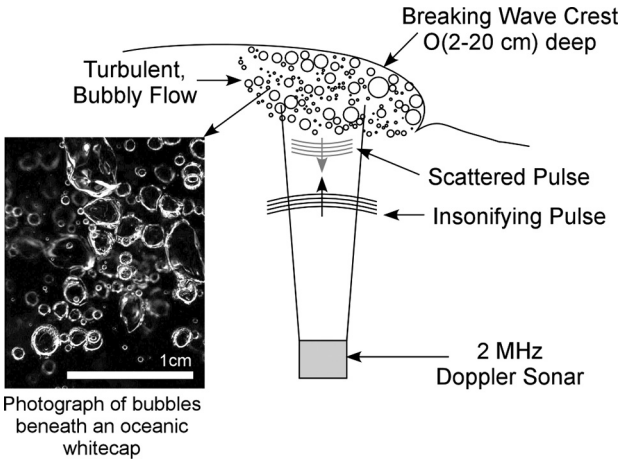

Fig. 1. Geometry for the scattering calculations. A 2-MHz Doppler sonar is mounted beneath the sea surface pointing into an actively breaking wave crest. Energy scattered from an insonifying pulse by the bubble plume within the wave crest is received and analyzed by the sonar. The picture on the left-hand side shows bubbles within a breaking, oceanic wave crest.

The study of bubble clouds by sonar dates back to the 1980s whereas the study of bubble plumes with sonar is a relatively new endeavor.

An absolute limiting range for sonar performance is presented by the sea surface, which represents an impenetrable barrier beyond which no information can be gained. Since the sea surface is equivalent to a bubble plume for which the air fraction $\alpha = 1$, and since air fractions in bubble plumes can reach values as high as 0.6 in the field [4], the questions naturally arise: At what air fraction does a plume become impenetrable to high-frequency Doppler sonar acoustic pulses and can these pulses be used to remotely probe the interior of actively breaking wave crests?

Here we present model calculations of the acoustic backscatter and extinction cross sections of characteristic bubble plumes entrained by actively breaking wave crests, and use them to compute limits on high-frequency Doppler sonar performance. The results depend somewhat on the assumptions made about the size distributions of bubbles within the plume, but a relatively robust conclusion can be drawn from the calculations. High-frequency sonars begin to degrade significantly in performance for air fractions in the range 0.03–0.06 and become inoperable for air fractions in the range 0.08–0.17.

II. Model Calculations

The geometry for the model calculations is shown in Fig. 1. A 2-MHz Doppler sonar transmits an insonifying acoustic pulse into a bubble plume created by an actively breaking wave crest. The bubble plume is assumed to extend O(2-20 cm) beneath the instantaneous sea surface and contain bubbles of radius 0.06–6 mm. The photograph on the left-hand side of Fig. 1 shows bubbles within an oceanic plume, taken with a video camera mounted on a surface-following frame off the Martha's Vineyard Air–Sea Interaction Tower during a winter storm in November 2008. This photograph illustrates the fundamental problem. Despite the narrow depth of field of the picture—O(5 mm)—the geometrical cross section of the bubbles occupies roughly 1/3 of the image. The presence of large bubbles packed together leads to high extinction rates at high acoustic frequencies where geometrical scattering dominates. For the model calculations the bubble plume is assumed to persist for O(1 s) or less and contain air fractions up to 0.6. Assumptions made about bubble size distribution and air fraction are discussed in greater detail below. Bubbles in the insonified plume are assumed to scatter some fraction of the insonifying pulse back to the sonar transceiver, where it is time gated and processed for scattering amplitude and Doppler shift.

The sonar pulse decreases in amplitude as it propagates through the water column because of geometrical spreading, absorption by the water, and scattering by bubbles. The amplitude of the signal returned to the sonar through backscatter is a function of the pulse amplitude versus range and the differential backscatter cross section of the scattering centers. The Doppler shift of the backscattered signal depends on the velocity of the scattering centers projected in the direction of the insonifying signal. Since the insonifying and backscattered pulse follow the same path, it is the roundtrip attenuation that determines the backscatter pulse amplitude at the sonar transceiver. Two quantities need to be computed to determine the sonar performance: the extinction cross section, which controls sound absorption, and the differential backscattering cross section, which controls backscatter amplitude.

The theory for acoustic backscattering and signal extinction through the bubble cloud employed here is based on Foldy's theory for the multiple scattering of waves [17], with allowance for anisotropic scattering [18]. Foldy showed that the total sound field in a cloud of isotropic scattering centers can be separated into two components corresponding to coherent and scattered sound fields. The calculations presented here are limited to the coherent field and show that this is so rapidly attenuated by bubble scattering and absorption that the concept of a coherent Doppler sonar pulse propagating through a bubble plume rapidly breaks down in high air fraction plumes. In this case, the calculation of a coherent backscatter signal becomes moot.

Using Foldy's theory, the coherent field is found by solving the wave equation for a continuous but lossy medium whose properties are determined by weighted integrals of the isotropic scattering coefficient $g(a, \omega)$, which is a function of bubble radius a and angular frequency ω [17]. To put the scattering coefficient into a more widely understood context, it is related to the total scattering cross section through $\sigma_s = 4\pi|g|^2$ and the extinction cross section through $\sigma_e = -4\pi \mathrm{Im}(g)/k$, where k is the wave number of the incident plane wave in the bubble-free medium. As Foldy states in his 1945 paper, this simple picture is applicable only when the number of scatterers per unit volume is sufficiently small [17]. Otherwise, there is interference between the scatterers and they no longer can be considered to absorb and scatter independently.

Foldy's theory assumes that scattering centers are isotropic, which is accurate for $ka \ll 1$, where a is bubble radius. For sonar frequencies in the megahertz range, $ka > 1$ for the mm-scale bubbles found in breaking crests and scattering from these bubbles lies in the geometrical scattering regime, which

is anisotropic. Moreover, the bubble density in breaking wave crests is so high that Foldy's approximation of replacing the external field acting on the jth scatterer averaged over all configurations of the other scatterers by the average field which would exist at the position of the jth scatterer when the scatterer is not present is inaccurate. In this case, multiple scattering effects can be expected to be important.

Notwithstanding the limitations of applying Foldy's theory to $ka > 1$ scattering and high air fractions, we will show that the absorption of high-frequency sound by oceanically relevant bubble plumes is so high that inaccuracies in Foldy's formulation are unlikely to change the substance of our final conclusions.

A. Acoustic Absorption by the Bubble Plume

Acoustic energy propagating through a bubble plume is lost through scattering by bubbles, and through conversion of sound to heat by viscous and thermal dissipation. From Foldy's theory, the flux of energy in a plane wave is reduced by the factor $\exp(-S_e)$ per unit distance, where the extinction cross section per unit volume is given by [17]

$$S_e = \int_{a_{\min}}^{a_{\max}} \sigma_{e,\text{full}}(a,\omega) n(a) da \tag{1}$$

where $\sigma_{e,\text{full}}$ is the asymptotically valid extinction cross section discussed below, a is bubble radius, which lies in the range $a_{\min} \le a \le a_{\max}$, and $n(a)$ is the density of scattering centers with dimensions of number of centers per unit volume per unit radius increment. Note that in the ocean acoustic literature, the standard units for $n(a)$ are bubbles per unit volume per micrometer radius increment, which is a factor of 10^{-6} smaller. Equation (1) is based on the extinction theorem presented for the multiple scatter of waves presented by Waterman and Truell [18], which leads to the additive rule for cross sections valid for sufficiently low densities of anisotropic scatterers. The criterion stated by Waterman and Truell is that the average pressure field exciting a bubble must be greater than the pressure wave scattered by a neighboring bubble, which for a monodisperse population of bubbles can be written

$$\frac{n\sigma_s}{k} \ll 1 \tag{2}$$

where n is the number of bubbles per unit volume, σ_s is the total scattering cross section, and k is the acoustic wave number. This criterion can be generalized to a polydisperse population of bubbles through the requirement that

$$\frac{1}{k}\int \sigma_s n da \ll 1. \tag{3}$$

This requirement was checked and found to be satisfied for the three bubble populations, two frequencies and range of air fractions studied here.

The bubble extinction cross section σ_e for $ka \ll 1$ is well known (e.g., [19] corrected by a factor of 2 and [20])

$$\sigma_e = \frac{8\pi\beta a c \omega^2}{\left(\omega_0^2 - \omega^2\right)^2 + 4\beta^2\omega^2}, \qquad ka < 1 \tag{4}$$

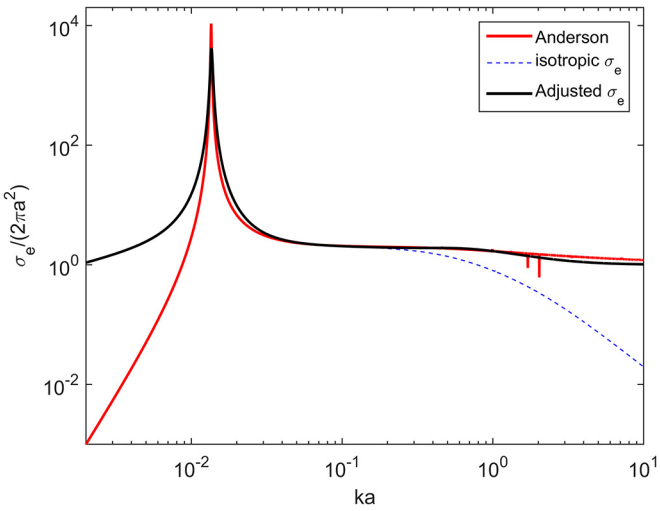

Fig. 2. Bubble extinction cross section as a function of ka. Anderson's anisotropic theory is plotted in red and does not include thermal and viscous damping, which gives rise to large differences between the correct, isotropic theory and Anderson's expression for $ka \ll 1$. The isotropic theory given by (2) is plotted in blue. The black line calculated using (3) shows an adjusted version of the isotropic theory that yields the correct geometrical extinction cross section for large ka and accounts for thermal and viscous losses for $ka \ll 1$.

where β is the dimensional damping factor, which includes viscous, thermal, and radiation losses; ω_0 is the bubble natural frequency, which is a function of bubble radius, surface tension, and water depth; and c is the speed of sound in the water. For $\omega \sim \omega_0$, the extinction cross section can be very large, an observation that has been verified by direct measurement of absorption by high air fraction bubble plumes in the surf zone [21] and transmission through these plumes [22]. In this regard, Gemmrich's choice to use a sonar in the megahertz frequency range to probe whitecap interiors is well considered since it shifts scattering away from bubble resonance, where absorption is high, and into the geometrical regime [10].

Equation (2) is accurate for $ka \ll 1$, but does not asymptote to the well-known geometrical limit of $2\pi a^2$ as $ka \to \infty$. Thuraisingham [23] and Zhang [24] have developed expressions for scattering cross section which could be used to extend the validity of σ_e to values of $ka \sim O(1)$. However, we require an expression for the extinction cross section valid for $ka \gg 1$. A version of (2) valid in the asymptotic limit $ka \to \infty$ can be found by adding a power law function of ka that has the correct limiting value

$$\sigma_{e,\text{full}} = \sigma_e + \frac{(ka)^{\alpha_e}}{\beta_e + (ka)^{\alpha_e}} 2\pi a^2. \tag{5}$$

The constants $\alpha_e = 2.9$ and $\beta_e = 0.12$ are determined as follows. Anderson [25] has presented a fully anisotropic theory for acoustic scattering by a fluid sphere. Anderson's model is valid for $ka > 1$, but not $ka \ll 1$ as it does not account for thermal and viscous losses in the bubble response around resonance. Values for α_e and β_e are determined from a least mean squares fit between $\sigma_{e,\text{full}}$ calculated using (5) and Anderson's theory over the range $0.1 \le ka \le 10$, resulting in an expression that is asymptotically valid in both limits $ka \ll 1$ and $ka \gg 1$. Values of $\sigma_{e,\text{full}}$ are plotted in Fig. 2 along with Anderson's theory

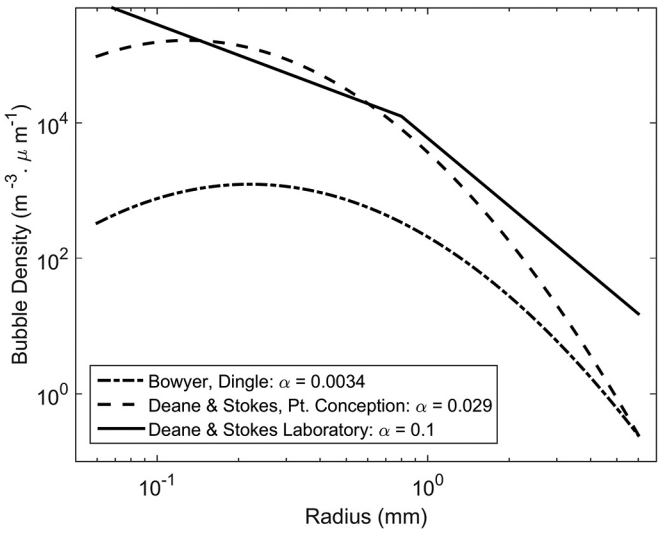

Fig. 3. Bubble size distributions chosen to be representative of bubble plumes. Dashed–dotted line: a distribution measured by Bowyer in Dingle Harbor [8]. Broken line: a distribution measured beneath a breaking wave crest 160 km west of Point Conception in 2001 [9]. Solid line: a laboratory distribution representative of plunging breakers [9]. All distributions are for waves breaking in salt water.

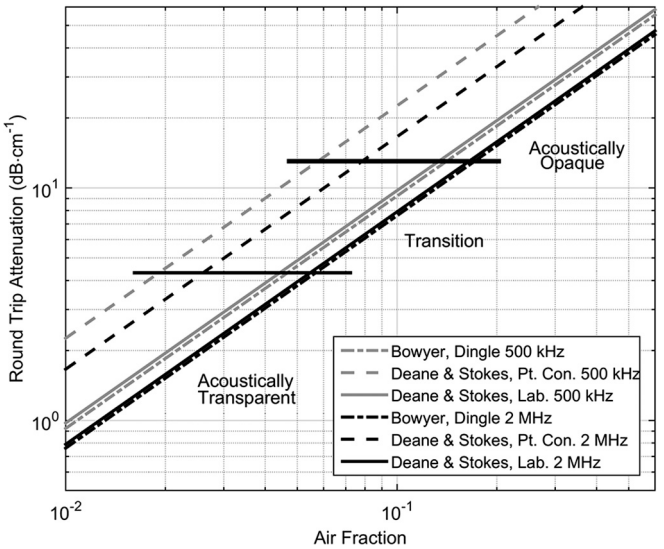

Fig. 4. Bubble plume extinction expressed in units of roundtrip attenuation in dB $\cdot$ cm^{-1} as a function of air fraction for the three size distributions plotted in Fig. 4. Short, horizontal lines have been drawn for roundtrip attenuation values corresponding to $\exp(-1)$ and $\exp(-3)$. Curves are shown for 500 kHz and 2 MHz.

and (2) as a function of ka. The curves have been normalized by the value of the absorption cross section in the geometrical limit $ka \to \infty$, which is $2\pi a^2$. A bubble of radius $a = 1$ mm placed at the sea surface was used to compute the dimensional damping factor β according to the equations in [19].

Equation (3) can be used to compute the plane wave extinction rate within an actively breaking crest once $n(a)$ is specified. We have investigated three functional forms for $n(a)$, and these are shown in Fig. 3. Two of the chosen distributions were measured during wave breaking at sea, and a third is a distribution from [9] reported to be representative of bubble plumes generated by plunging laboratory breaking waves in salt water. The smallest and largest bubbles in the distributions were chosen to be 60 μm and 6 mm, respectively. This is the range of bubble sizes reported by Bowyer [8], which is also consistent with the oceanic observations of Deane and Stokes [9].

For the model study, the three distributions were uniformly scaled to yield a chosen air fraction, allowing calculation of the acoustic attenuation as a function of α. Air fraction was assumed to lie in the range 0.01–0.6, the upper limit representing the highest values of air fraction observed in actively breaking crests at sea [4]. Air fractions exceeding 0.5 in laboratory breaking waves have also been reported by Lamarre and Melville [3] and Blenkinsopp and Chaplin [5].

The attenuation curves calculated by substituting (5) for $\sigma_{e,\mathrm{full}}$ into (1) are shown for the three chosen bubble distributions in Fig. 4 as a function of air fraction. The attenuation is plotted as roundtrip attenuation in dB $\cdot$ cm^{-1}. A roundtrip attenuation of 10 dB $\cdot$ cm^{-1} means that a plane wave penetrating the base of the plume and scattered by a layer of bubbles 1 cm from the base of the plume is attenuated by 10 dB during its roundtrip from the bubble layer and back out again. The attenuation is multiplicative with propagation path length, so the same plane wave scattered from bubbles 10 cm into the plume is attenuated by 100 dB.

The short, horizontal lines in Fig. 4 show attenuation values corresponding to roundtrip attenuations of $\exp(-1)$ and $\exp(-3)$. These values are somewhat arbitrarily chosen to represent the transition from what we are calling an "acoustically transparent" to an "acoustically opaque" plume. Roundtrip attenuations of $\exp(-1)$ and $\exp(-3)$, respectively, correspond to losses of 43 and 130 dB from signals scattered 10 cm upward from the base of a bubble plume. We are assuming here that 130 dB of signal attenuation is more than any real sonar system can accommodate.

The Dingle Harbor and laboratory distributions yield very similar attenuations, which transition from acoustically transparent to opaque over a higher range of air fractions than the Point Conception distribution. Taking the range of air fraction indicated for a given level of absorption, our model calculations suggest that 2-MHz sonars will degrade significantly in performance for air fractions in the range 0.03–0.06 (the upper end of the transparent region) and become completely inoperable for air fractions in the range 0.08–0.17 (the lower end of the opaque region). The higher acoustical absorption at 500 kHz causes the operating regime shift to occur at slightly lower air fractions, making the overall situation worse. The calculations presented here neglect multiple scattering effects, which tend to increase acoustic absorption [26], and so these numbers should be considered as conservative estimates for performance.

B. Doppler Shift Bias by Bubbles in the Plume

A second effect that degrades the performance of high-frequency Doppler sonars pointed at breaking wave crests is the Doppler shift associated with the motion of large bubbles. One of the assumptions made when analyzing backscatter

returns from Doppler sonars is that the scattering centers giving rise to the backscatter signal are Lagrangian tracers, i.e., they move with the fluid. This is often a reasonable assumption. For example, a 100-kHz sonar operating near the sea surface will generate resonant returns from bubbles approximately 32 μm in radius, which have a rise velocity of only $\sim$2 mm $\cdot$ s^{-1}. Moreover, when using Doppler signals to estimate fluid turbulent dissipation rate, bubbles rising uniformly will add a constant bias to fluid velocity that will be processed out when velocity spectra are calculated. For these examples, using Doppler sonars to investigate coherent and turbulent fluid motions in the upper ocean boundary layer can be justified. The situation is not the same for high air fraction bubble plumes remotely sensed with high-frequency Doppler sonars. As discussed earlier, scattering in bubble plumes is dominated by geometrical scattering, not bubble resonant scattering (although the possibility of resonant scattering is discussed further in the discussion section). As shown below, in this regime, much of the backscatter signal originates from large bubbles with relatively high buoyant rise speeds that interact with fluid turbulence, which significantly complicates the interpretation of measured Doppler shift.

The bias introduced by the buoyant rise of large bubbles can be estimated by calculating the differential backscatter cross section as a function of bubble radius. Just as the extinction cross section describes the absorption of coherent energy propagating through the plume, the differential backscatter cross section describes the amplitude of a backward-propagating signal generated by bubbles in a control volume. Following the same computation method used to generate a uniformly valid expression for the extinction cross section, the differential backscattering cross section can be written as

$$\Delta\sigma_{bs,\text{full}} = \Delta\sigma_{bs} + \frac{(ka)^{\alpha_{bs}}}{\beta_{bs} + (ka)^{\alpha_{bs}}} \frac{a^2}{4} \tag{6}$$

where the constants $\alpha_{bs} = 4.2$ and $\beta_{bs} = 28$ were determined to yield a least mean squares difference fit to the anisotropic theory of Anderson [25] over the range $0.1 \leq ka \leq 10$ and the differential backscattering cross section is given by $\Delta\sigma_{bs} = \sigma_s/4\pi$ where

$$\sigma_s = \frac{4\pi a^2}{(1 + k^2a^2)\left(\left(\omega_0^2/\omega^2 - 1\right)^2 + 4\beta^2/\omega^2\right)}, \qquad ka < 1. \tag{7}$$

When multiplied by the bubble size distribution and integrated over bubble size, $\Delta\sigma_{bs}$ yields the total backscatter cross section.

The contribution of bubbles of various sizes to backscatter can be determined from Fig. 5, which shows the cumulative, fractional contribution to the total backscatter cross section as a function of bubble radius. As with all normalized, cumulative distributions, the curves in Fig. 5 begin with a value of 0 and end with a value of 1. For the Point Conception distribution, 1/2 of the total backscatter comes from bubbles larger than $\sim$0.6 mm radius. For the laboratory and Dingle Harbor distributions, 1/2 of the backscatter originates from bubbles with radius

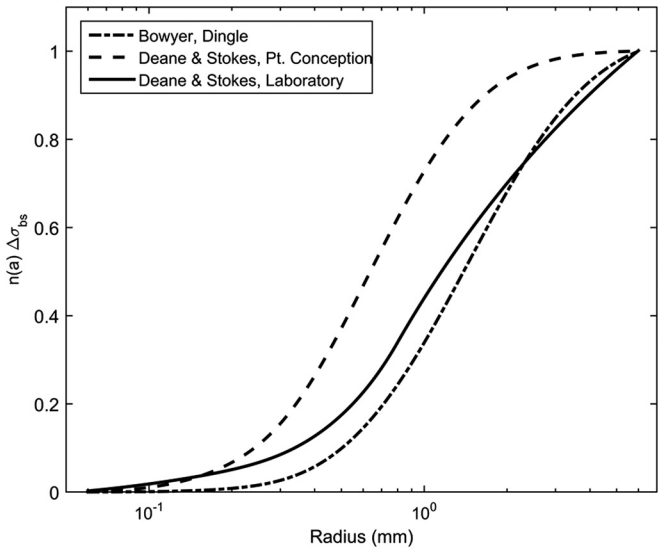

Fig. 5. Normalized, cumulative differential backscatter cross section, multiplied by bubble size distribution and integrated as a function of bubble radius, calculated at 2 MHz.

lying in the range 1.2–1.4 mm. The terminal velocity of bubbles 0.6 mm and larger lies in the range 15–25 cm $\cdot$ s^{-1} [27], which represents a significant source of velocity bias.

Furthermore, the strong bias introduced by bubble buoyancy effects cannot be processed out when producing velocity spectra because the interactions between large bubbles and turbulent fluid flow cannot be neglected in bubble plumes. Spelt and Biesheuvel [28] explored bubble–turbulence interaction with theory and showed how fluctuations in one component of the lateral vorticity causes bubbles to move under the action of lift forces in the other lateral direction, toward regions where the difference between bubble and fluid velocity is largest. Mean bubble rise speeds relative to those in quiescent water were numerically determined for different turbulent intensities β_{SB} (with β_{SB} the ratio between the turbulence intensity and the bubble rise velocity in still fluid) and found to decrease by up to 35%–50% depending on the turbulence model used. Laboratory studies of Poorte and Biesheuvel [29] generally confirmed the numerical predictions. Although finding somewhat smaller changes in mean bubble rise speed, they did observe turbulence-induced deviations from still fluid terminal velocity on the order of 0.4, or up to $\sim$10 cm $\cdot$ s^{-1} for oceanic bubble plumes. Since 1/2 of the backscatter signal generated comes from large bubbles subject to interactions with turbulence, random velocity fluctuations on the order of 10 cm $\cdot$ s^{-1} will be introduced into the turbulence velocity spectra which will tend to increase the fluid turbulence dissipation rate attributed to the bubble plume. This effect will occur independently of acoustic absorption by the plume, and will thus present a problem whether the plume is acoustically transparent or not.

III. Discussion

The first obstacle encountered using high-frequency ($>$ 500 kHz) Doppler sonars to quantify turbulence in actively breaking wave crests is the extinction of sound by bubbles.

Large bubbles and high-frequency signals result in a geometrical scattering regime, which is beneficial because bubble resonant scatter is eliminated. However, the high air fractions encountered in actively breaking oceanic wave crests still limit the penetration depth high-frequency sonar signals to O(1 cm) for air fractions greater than roughly 0.1, which is the order of air fraction at the end of active breaking but not during active breaking when air fractions can be as high as 0.6. After active breaking ceases, turbulence levels decay and large bubbles are rapidly lost to buoyancy-driven degassing. These conditions are consistent with the acoustically transparent regime identified in Fig. 5, and high-frequency sonar performance should not be compromised when operated over O(m) ranges once the bubble plume has degassed.

Our conclusions regarding acoustical absorption in the geometrical scattering regime are consistent with the observation that the interior of high air fraction bubble plumes cannot be studied using the scatter of light. Since light scattering from bubbles in plumes largely occurs in the geometrical scattering regime, Fig. 4 applies to optical scattering and optical path lengths in plumes are limited to O(1 cm) for high air fraction plumes. For example, digital particle imaging velocimetry, which requires the illumination of fluorescent tracer particles in the interior of bubble plumes with lasers, is limited to non-aerated flow or dilute bubble flow beneath the wave trough level [30].

The backscatter cross-section calculations show that even if high-frequency acoustic signals were able to penetrate a significant distance into the interior of actively breaking wave crests, a significant fraction of the signal observed would be from large bubbles, whose terminal velocities are altered by the presence of the fluid turbulence under study. The random nature of these velocity fluctuations will be a measure of bubble–turbulence interactions, not the turbulence itself and the interpretation of such signals would require an accounting of these interactions. The significant bias introduced by scattering from large bubbles will play an important role in the Doppler shifts encountered in signals scattered from the base of bubble plumes, complicating estimates of fluid turbulence there.

A possible resolution to the bias problem would be the presence of a sufficiently large number of resonant bubbles. If present, these bubbles could dominate the backscatter signal through resonant scattering, reducing the bias introduced by large bubbles. Resonant scattering at 2 MHz implies a bubble radius of ~ 2 μm, and such small bubbles cannot remain in suspension for long as surface tension rapidly drives them into solution. In the event that bubbles of this scale were stabilized by coatings of surface-active material, and thus were able to build up in concentration over time in the upper ocean boundary layer, then their resonant contribution to scattering will also increase the acoustic absorption rate, leading to further reductions in acoustic penetration beyond those shown in Fig. 4 and a more rapid transition from an acoustically transparent to acoustically opaque regime. Thus, an increase in the population of resonant bubbles will not improve the overall situation. Finally, it should be noted that there is little to gain by reducing the sonar frequency as this will only increase the extinction rate as the resonance frequency of small bubbles is approached, as the calculations at 500 kHz show.

IV. Concluding Remarks

We have performed model calculations of the acoustical absorption and backscatter of high-frequency Doppler sonar signals from high air fraction, oceanic bubble plumes encountered within actively breaking wave crests. The calculations are based on observed oceanic bubble distributions, scaled to a range of air fractions consistent with field observations and the development of asymptotically uniform expressions for the extinction and backscattering cross sections valid in the geometrical scattering limit. The factor responsible for high signal absorption is the high air fraction encountered in breaking wave crests, not the high acoustical frequencies considered in the model calculations. Studies of bubble clouds with typical air fractions of 10^{-4} and less using high-frequency Doppler sonars are not likely to be rendered inoperable by excessive bubble scatter, although absorption of sound as it propagates through the cloud should be properly accounted for when calculating bubble backscatter cross sections [31].

Drawing from these calculations, we have identified a transition in propagation behavior for high-frequency (500 kHz–2 MHz) sonar signals in bubble plumes, from an acoustically transparent regime, with roundtrip absorption of $\exp(-1)$ and less per centimeter, to an acoustically opaque regime with absorption of $\exp(-3)$ and more per centimeter. At 2 MHz, the transition occurs over an air fraction range of 0.03–0.17, which is at the low end of the range encountered in actively breaking crests. We note here that the amplitude of a backscattered probe signal with unit amplitude initially and propagating through 10 cm of plume with an absorption rate of $\exp(-1)$ per centimeter is $\exp(-10) \sim 5 \times 10^{-5}$. Consequently, the value of our transitional range of air fraction between propagation regimes should be considered conservative.

Our model calculations suggest that the interpretation of backscattered acoustic signals from bubbles plumes in actively breaking wave crests in terms of fluid turbulence are problematic, and the best option currently available for studying these energetic, aerated flows is still *in situ* observation. We also acknowledge that these are model calculations, and laboratory experiments are called for to test the operation of high-frequency Doppler sonars when used to probe the interior of actively breaking waves.

Acknowledgment

The author would like to thank Dr. D. Farmer for insightful observations that improved the content of this paper, and Dr. J. Gemmrich for a number of helpful discussions.

References

[1] W. K. Melville, "The role of surface wave breaking in air-sea interaction," *Annu. Rev. Fluid. Mech.*, vol. 28, pp. 279–321, 1996.

[2] M. D. Stokes, G. B. Deane, M. I. Latz, and J. Rohr, "Bioluminescence imaging of wave-induced turbulence," *J. Geophys. Res.*, vol. 109, 2004, DOI: 10.1029/2003JC001871.

[3] E. Lamarre and W. K. Melville, "Air entrainment and dissipation in breaking waves," *Nature*, vol. 351, pp. 469–472, 1991.
[4] J. R. Gemmrich and D. M. Farmer, "Observations of the scale and occurrence of breaking surface waves," *J. Phys. Oceanogr.*, vol. 29, pp. 2595–2606, 1999.
[5] C. E. Blenkinsopp and J. R. Chaplin, "Void fraction measurements in breaking waves," *Proc. R. Soc. A*, vol. 463, pp. 3151–3170, 2007.
[6] M. D. Anguelova and P. Huq, "Characteristics of bubble clouds at various wind speeds," *J. Geophys. Res.*, vol. 117, 2012, DOI: 10.1029/2011JC007442.
[7] V. S. Bezzabotnov, R. S. Bortkovskii, and D. F. Timanovskii, "On the structure of the two-phase medium generated at wind-wave breaking," *Izvestiya Akademii Nauk SSSR, Fizika Atmosfery I Okeana*, vol. 22, pp. 1186–1193, 1986.
[8] P. A. Bowyer, "Video measurements of near-surface bubble spectra," *J. Geophys. Res.*, vol. 106, pp. 14179–14190, 2001.
[9] G. B. Deane and M. D. Stokes, "Scale dependence of bubble creation mechanisms in breaking waves," *Nature*, vol. 418, pp. 839–844, 2002.
[10] J. R. Gemmrich, "Strong turbulence in the wave crest region," *J. Phys. Oceanogr.*, vol. 40, pp. 583–595, 2010.
[11] S. A. Thorpe and A. J. Hall, "The characteristics of breaking waves, bubble clouds, and near-surface currents observed using side-scan sonar," *Continental Shelf Res.*, vol. 1, pp. 353–384, 1983.
[12] R. Pinkel and J. A. Smith, "Open ocean surface wave measurement using Doppler sonar," *J. Geophys. Res.*, vol. 92, C12, pp. 12967–12973, 1987, DOI: 10.1029/JC092iC12p12967.
[13] S. Vagle and D. M. Farmer, "The measurement of bubble-size distributions by acoustical backscatter," *J. Atmosph. Ocean. Technol.*, vol. 9, pp. 630–644, 1992.
[14] M. V. Trevorrow, "Measurements of near-surface bubble plumes in the open ocean with implications for high-frequency sonar performance," *J. Acoust. Soc. Amer.*, vol. 114, pp. 2672–2684, 2003.
[15] A. D. Graham, K. Woolf, and A. J. Hall, "Aeration due to breaking waves. Part I: Bubble populations," *J. Phys. Oceanogr.*, vol. 34, pp. 989–1007, 2004.
[16] M. J. Ulloa, "Interpreting underwater acoustic images of the upper ocean boundary layer," *Eur. J. Phys.*, vol. 28, pp. 301–309, 2007, DOI: 10.1088/0143-0807/28/2/015.
[17] L. L. Foldy, "The multiple scattering of waves. I. general theory of isotropic scattering by randomly distributed scatterers," *Phys. Rev.*, vol. 67, pp. 107–119, 1945.
[18] P. C. Waterman and R. Truell, "Multiple scattering of waves," *J. Math. Phys.*, vol. 2, pp. 512–537, 1961.
[19] A. Prosperetti, "Thermal effects and damping mechanisms on the forced radial oscillations of gas bubbles in liquids," *J. Acoust. Soc. Amer.*, vol. 61, pp. 17–27, 1977.
[20] A. A. Ainslie and T. G. Leighton, "Review of scattering and extinction cross-sections, damping factors, and resonance frequencies of a spherical gas bubble," *J. Acoust. Soc. Amer.*, vol. 130, pp. 3184–3208, 2011.
[21] G. B. Deane, "Acoustic hot-spots and breaking wave noise in the surf zone," *J. Acoust. Soc. Amer.*, vol. 105, pp. 3151–3167, 1999.
[22] D. M. Farmer, G. B. Deane, and S. Vagle, "The influence of bubble clouds on acoustic propagation in the surf zone," *IEEE J. Ocean. Eng.*, vol. 26, no. 1, pp. 113–124, Jan. 2001.
[23] R. A. Thuraisingham, "New expressions of acoustic cross-sections of a single bubble in the monopole bubble theory," *Ultrasonics*, vol. 35, pp. 407–409, 1997.
[24] Y. Zhang, "A generalized equation for scattering cross-section of spherical gas bubbles oscillating in liquids under acoustic excitation," *J. Fluids. Eng.*, vol. 135, 2013, DOI: 10.1115/1.4024128.
[25] V. C. Anderson, "Sound scattering from a fluid sphere," *J. Acoust. Soc. Amer.*, vol. 22, pp. 426–431, 1950.
[26] Z. Ye, L. Ding, and L., "Acoustic dispersion and attenuation relations in bubbly mixture," *J. Acoust. Soc. Amer.*, vol. 98, pp. 1629–1636, 1995.
[27] L. S. Fan and K. Tsuchiya, *Bubble Wake dynamics in Liquids and Liquid-Solid Suspensions*, Chemical Engineering London, U.K.: Butterworth-Heinemann, 1990, p. 363.
[28] P. D. M. Spelt and A. Biesheuvel, "On the motion of gas bubbles in homogeneous isotropic turbulence," *J. Fluid. Mech.*, vol. 336, pp. 221–244, 1997.
[29] R. E. G. Poorte and A. Biesheuvel, "Experiments on the motion of gas bubbles in turbulence generated by an active grid," *J. Fluid. Mech.*, vol. 461, pp. 127–154, 2002.
[30] Y. Watanabe, Y. Hideshima, T. Shigematsu, and K. Takehara, "Application of three-dimensional hybrid stereoscopic particle image velocimetry to breaking waves," *Measur. Sci. Technol.*, vol. 17, no. 6, pp. 1456–1469, 2006, DOI: 10.1088/0957-0233/17/6/025.
[31] S. Vagle, and D. M. Farmer, "A comparison of four methods for bubble size and void fraction measurements," *IEEE J. Ocean. Eng.*, vol. 23, no. 3, pp. 211–222, Jul. 1998.

Grant Deane received the B.Sc. and M.Sc. degrees in physics (honors) from Auckland University, Auckland, New Zealand, in 1982 and 1983, respectively and the D.Phil. degree in mathematics from Oxford University, Oxford, U.K., in 1989.

He was a Mellon Fellow at Scripps Institution of Oceanography, University of California San Diego (UCSD), La Jolla, CA, USA, from 1990 to 1992. He has been a Research Oceanographer at SIO since 1995 and is the Director of the SIO Hydraulics Laboratory. His research interests include underwater acoustics, small-scale, upper ocean physics (wave breaking, turbulence, air entrainment, and marine aerosol generation), and bioluminescence.

Dr. Deane is a Fellow of the Acoustical Society of America and a member of the American Geophysical Union and the American Meteorological Society. He is currently an Associate Editor for the *Journal of the Acoustical Society of America Express Letters*.